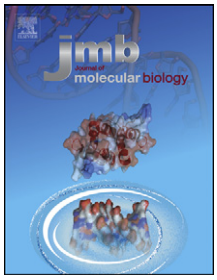

3D Cryo-Electron Reconstruction of BmrA, a Bacterial Multidrug ABC Transporter in an Inward-Facing Conformation and in a Lipidic Environment

Pierre Frederic Fribourg[1,2], Mohamed Chami[3], Carlos Oscar S. Sorzano[4], Francesca Gubellini[1,2], Roberto Marabini[4], Sergio Marco[1,5], Jean-Michel Jault[6] and Daniel Lévy[1,2,7]

*1 - **Institut Curie,** Centre de Recherche, 26 rue d'Ulm, 75231 Paris, France*
*2 - **CNRS,** UMR 168, 11 rue Pierre et Marie Curie, 75231 Paris, France*
*3 - **Center for Cellular Imaging and NanoAnalytics,** Biozentrum, University Basel, Mattenstrasse 26, CH-4058 Basel, Switzerland*
*4 - **Centro Nacional de Biotecnología,** Unidad de Bioinformática, Campus Universidad Autónoma (Cantoblanco), 28049 Madrid, Spain*
*5 - **Institut Curie,** Centre de Recherche, Inserm, U759, Centre Universitaire d'Orsay, Bâtiment 112, Orsay 91405, France*
*6 - **Institut de Biologie Structurale,** UMR 5075, Université Joseph Fourier/CEA/CNRS, 41 rue Jules Horowitz, 38027 Grenoble Cedex 1, France*
*7 - **The BioImaging Cell and Tissue Core Facility,** Institut Curie, 75231 Paris, France*

***Correspondence to Jean-Michel Jault and Daniel Lévy:** D. Lévy, Institut Curie, UMR 168, 11 rue Pierre et Marie Curie, 75231 Paris Cedex 05, France. jean-michel.jault@ibcp.fr; daniel.levy@curie.fr*
http://dx.doi.org/10.1016/j.jmb.2014.03.002
Edited by J. Bowie

Abstract

ABC (*A*TP-*b*inding *c*assette) membrane exporters are efflux transporters of a wide diversity of molecule across the membrane at the expense of ATP. A key issue regarding their catalytic cycle is whether or not their nucleotide-binding domains (NBDs) are physically disengaged in the resting state. To settle this controversy, we obtained structural data on BmrA, a bacterial multidrug homodimeric ABC transporter, in a membrane-embedded state. BmrA in the apostate was reconstituted in lipid bilayers forming a mixture of ring-shaped structures of 24 or 39 homodimers. Three-dimensional models of the ring-shaped structures of 24 or 39 homodimers were calculated at 2.3 nm and 2.5 nm resolution from cryo-electron microscopy, respectively. In these structures, BmrA adopts an inward-facing open conformation similar to that found in mouse P-glycoprotein structure with the NBDs separated by 3 nm. Both lipidic leaflets delimiting the transmembrane domains of BmrA were clearly resolved. In planar membrane sheets, the NBDs were even more separated. BmrA in an ATP-bound conformation was determined from two-dimensional crystals grown in the presence of ATP and vanadate. A projection map calculated at 1.6 nm resolution shows an open outward-facing conformation. Overall, the data are consistent with a mechanism of drug transport involving large conformational changes of BmrA and show that a bacterial ABC exporter can adopt at least two open inward conformations in lipid membrane.

Introduction

ABC (*A*TP-*b*inding *c*assette) transporters form one of the largest families of membrane proteins involved in import or export of a large diversity of substrates in all living organisms. In human, the dysfunction of several ABC transporters causes severe sicknesses including cystic fibrosis, adrenoleukodystrophy or hyperinsulinemia [1,2]. Other ABC transporters are involved in multidrug resistance phenotypes in cancer cells, notably the P-glycoprotein (P-gp), and related transporters are found in microorganisms, from protozoa to bacteria, and confer resistance toward medicinal treatments in pathogenic strains [3]. All ABC transporters share a similar minimal core with two transmembrane domains (TMDs) and two cytosolic nucleotide-binding domains (NBDs), either borne on separate polypeptides or fused together. Three-dimensional (3D) structures have been obtained for several ABC transporters and in different

conformations (see recent reviews [4–6]). ABC importers show a rather compact organization, and the 3D structures solved in apostates and nucleotide-bound states suggest a mechanism where the NBDs remain engaged throughout the catalytic cycle [4,6].

In the case of ABC exporters, a common mechanism of drugs transport is not yet settled because (i) although conformations of a multidrug transporter with bound inhibitors have been solved, a structure with transported drugs is still lacking [7] and because (ii) of the controversy regarding the physiological relevance of the 3D structures of the open apo-conformation. Compared to ABC importers, the connection between NBDs and TMDs in ABC exporters is secured by two long intracellular domains (ICDs) that protrude from the TMDs and interact with the NBDs. As exemplified in the outward-facing conformation of the Sav1866 homodimer, ICD2 from one protomer interacts mainly with the NBD of the other protomer (*trans*-interaction) while ICD1 contacts primarily the NBD within the same protomer (*cis*-interaction) [8]. In this structure, the two NBDs are interacting together in a closed, ATP-bound, conformation. Three inward-facing (or open) conformations have been determined in the absence of nucleotides for *Escherichia coli* MsbA and P-gp from mouse and *Caenorhabditis elegans* [7,9,10] and in the presence of non-hydrolyzable nucleotide for human ABCB10 [11]. Moreover, three new inward-facing conformations of mouse P-gp with larger separation of the NBDs have been reported recently highlighting a large flexibility of the protein [12]. These apo-conformations revealed separated NBDs and a V-shaped structure in the transmembrane region that defines a large internal cavity that contains drugs binding sites. Accordingly, the ATP switch model for the transport cycle involves a large conformational change of protein that brings the NBDs in contact during the catalytic cycle (reviewed in Ref. [13]).

These open inward structures have nevertheless raised skepticism; they were proposed to reflect non-physiological states of the proteins possibly due to protein–protein interactions in the 3D crystals or to non-physiological states of the exporters in detergent micelles [14–17]. Moreover, the lack of significant conformational changes upon drug binding in the structure of mouse P-gp also raised questions since drugs increase or decrease ATPase activity [17,18]. Finally, the physiological relevance of the open apo-form is also questioned since the cellular ATP concentration (3–5 mM) exceeds the affinity of P-gp or MsbA for ATP (0.1–1 mM) and thus the nucleotide-free conformations may have a very transient existence. Therefore, alternative models (e.g., the constant contact model) have been proposed where the two NBDs of ABC exporters remain in contact throughout their catalytic cycle (recently reviewed in Ref. [14]). According to this mechanism, the cross-linking of the two cysteines residues located near the C-terminus of the NBDs of P-gp retained high level of drug stimulation of ATP hydrolysis suggesting the absence of large conformation motion of the NBDs during the ATP cycle [19]. An opposite conclusion was drawn from a recent study by luminescence resonance energy transfer (LRET) where NBDs of MsbA operate in association/dissociation mode under physiological conditions and possibly in a contact mode at lower temperatures [20].

On the other hand, significant proofs for the existence of open inward conformation have been derived from spectroscopic approaches, for example, double electron–electron resonance (DEER), LRET and fluorescence resonance energy transfer (FRET). MsbA was studied after spin labeling of amino acids at selected positions using DEER experiments and this transporter was shown to adopt in the resting state, an open conformation either in liposomes or nanodiscs [21–23] similar to that found in detergent and congruent with the open 3D structure obtained by X-ray crystallography [9]. Moreover, DEER experiments combined with molecular dynamic simulations have shown that P-gp adopts an unexpectedly wide range of apo-conformations, highlighted by the degree of separation between the two NBDs [24]. We have also studied BmrA, a bacterial homodimer from *Bacillus subtilis*, by hydrogen/deuterium exchange combined with mass spectroscopy and shown the high flexibility of the ICD domains of this transporter in the resting state [25].

These different models of functioning could reflect different mechanisms of transport by full-length eukaryotic or half-size bacterial transporters or are possibly related to the experimental approaches based on the use of local probes and sparse distance measurements. Electron paramagnetic resonance measurements combined with the Rosetta electron paramagnetic resonance method described the *de novo* determination of atomic structure of T4-lysozyme and αA-crystallin proteins [26]. This method has not been applied yet to ABC transporters and DEER, LRET or FRET distances have been derived from specific positions chosen in the atomic structures and with uncertainties on large distances as found between NBDs of MsbA in apostate [14,20,22].

This led us to analyze the apo-conformation of BmrA by cryo-electron microscopy (cryo-EM) and single particle analysis to provide a complete *de novo* envelope of another bacterial homodimeric ABC transporter embedded in a lipid bilayer. We previously reported a low-resolution 3D reconstruction obtained by cryo-EM of BmrA [27]. Here, using new sets of cryo-EM images, we calculated two new 3D models of BmrA where its subdomains and the

surrounding lipid bilayer are now unambiguously resolved. The NBDs of BmrA are clearly separated and the TMDs show a V-shaped conformation consistent with an open conformation similar to that found in the mouse P-gp X-rays structures. Furthermore, a second conformation of BmrA is found with the NBD more separated as reported for MsbA. Finally, two-dimensional (2D) crystals of the ATP-bound state revealed an outward-facing conformation of BmrA.

Results

Inward-facing conformation of apo-BmrA

BmrA was reconstituted in lipid membranes at a low lipid-to-protein ratio with egg phosphatidylcholine (EPC)/egg phosphatidic acid (EPA) lipid mixtures by detergent removal using Bio-Beads. Ring-shaped structures, thereafter named rings of BmrA, homogeneous in shapes and in sizes, were formed when the lipid bilayer was formed and the detergent to lipid below 1:1 molar ratio. Further elimination of detergent led to the coalescence of rings and the formation of non-crystalline tubes (Supplementary Material, Fig. S1). We have also previously shown that the rings of BmrA were preferentially oriented in top views in ice preventing the calculation of a 3D model. Side views were obtained after specific binding to a Ni^{2+}-NTA-DOGS lipid spread at the air water interface. These side views in combination with the *d*12 symmetry of the rings of BmrA allowed generating a complete 3D model [27]. The new preparation of rings of BmrA was then specifically bound to a Ni^{2+}-NTA-DOGS lipid layer spread at the air water interface. After transfer onto holey grids, circular and rectangular views of the rings were found (Fig. 1a, black arrows). Additional reconstituted material was also bound to the surface such as tubes or membrane sheets of different lengths and widths (white arrows).

After bi-dimensional classification and particles averaging, four main classes were extracted including two circular and two rectangular views (Fig. 1b–e). Particles depicted in Fig. 1b and d showed a 12 and 2 symmetries, respectively (Fig. S2). These particles were identical with the top and side views of the previously reported 3D model of *d*12 symmetry, respectively [27]. However, particles depicted in Fig. 1c and e were larger than the *d*12 particles and the bi-dimensional analysis revealed a *d*13 symmetry (Fig. S2).

The particles and their related symmetries were used to calculate 3D models of *d*12 and *d*13 rings at 2.3 and 2.5 nm resolution, respectively (Figs. S3 and S4). The *d*12 ring is 37.5 nm large and 13 nm thick and is made of 24 homodimers of BmrA (Fig. 2a). Although the increase of resolution of the new *d*12 3D model is modest, 2.3 nm *versus* 2.5 nm, the homodimers of BmrA and their different subdomains including the NBDs, the intracellular and the membrane domains are now better resolved compared to the previous 3D model [27] (Figs. 2b and 3b and Fig. S5). This is even more pronounced for the TMDs where two separated bundles of transmembrane densities and the two lipidic leaflets are now resolved (see also below). This allowed an unambiguous assignment of the homodimer of BmrA different from the previously erroneous assignment [27] (Fig. S5). The *d*13 ring is larger than the *d*12 ring, 39 nm large and 19 nm thick, and is made of 39 homodimers of BmrA (Fig. 2c).

In both rings, the overall shape of a BmrA homodimer corresponded to a V-shaped conformation with physically separated NBDs. The best global fit was obtained with the inward-facing structure of mouse P-gp (PDB ID: 3G5U) (Fig. 2b and d). The dimensions of BmrA are 11 nm height and 9.5 nm large at the level of the NBDs and the NBDs are separated by ~3 nm.

Within the membrane region, two separated and slightly tilted densities corresponding to the bundle of α-transmembrane helices were observed (Fig. 3). Moreover, two slightly curved layers of densities separated by 4 nm were visible along the ring and can be attributed to the phosphate densities of the polar head group of each lipidic leaflet of the bilayer (Fig. 3, arrows). The lipidic surface surrounding proteins was smaller at the inner leaflet (black arrows, extracellular side) than the outer leaflet (white arrows, cytoplasmic side). This difference and the V-shaped structure lead to the curvature of the membrane and the formation of homogeneous rings. It is worth noting that the electron density of the outer leaflet was weaker than the inner leaflet suggesting different composition and the presence of less electron dense residual molecules of detergent close to the cytoplasmic side.

We also analyzed the membrane tubes or sheets bound to the functionalized lipid layer that were homogeneous enough to perform a classification and 2D averaging (Fig. 4a). A first population was composed of thin membranes with a constant width of 17.5 nm and variable lengths between 20 nm and 50 nm. A 2D average shows that these membranes were made of layers of four circular densities aligned with 58° to the axis of the tube (Fig. 4b). This layer can be superimposed to the densities of the NBDs in the row in the *d*12 ring after a rotation from 58° to 38.5° to the axis of the ring (Fig. 4c). Moreover, the diameter of the densities of 4 nm was consistent with the size of a single NBD. This suggests that these membranes were also made of BmrA in an open conformation similar to the mouse apo-P-gp.

The second population was strikingly different from the previous one and made of membranes with a constant width of 25 nm and variable lengths between 20 nm and 300 nm (Fig. 4d and e). These

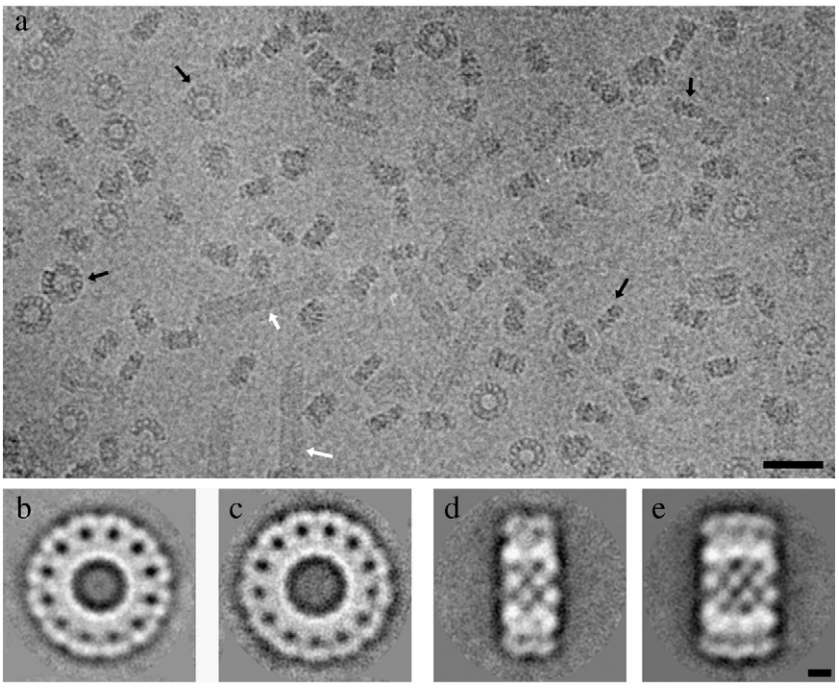

Fig. 1. Ring-shaped particles of BmrA reconstituted in lipid membrane after binding to a Ni^{2+}-NTA lipid layer. (a) Representative cryo-electron micrograph with circular or rectangular views of ring-shaped particles (black arrows). Other reconstituted structures such as tubes or membrane sheets were also present (white arrows). The micrograph has been 4-fold down-sampled to increase the contrast. The bar represents 25 nm. (b–e) Average images of the four mains classes of ring-shaped particles. The bar represents 5 nm.

membranes contained two identical rows with circular densities consistent with the size of a single NBD (Fig. 4d, rows numbered 1 and 2). However, the arrangement of the densities was different from the projection of the *d*12 ring. In order to understand the arrangement of BmrA in the membrane, we observed these tubes deposited on carbon-coated grids and after negative staining (Fig. 4e). The tubes were also of 25 nm width but were often twisted similar to a ribbon suggesting that they were flattened upon binding to the lipid layer. The twisted membranes revealed both sides of the membrane demonstrating that they were single membrane sheets rather than tubes (Fig. 4e). The NBDs pointing toward the outside were clearly visible revealing that BmrA was inserted in a single orientation in the membrane. This greatly facilitates the interpretation of the densities in the 2D averages of cryo-EM images (Fig. 4d). Two possible arrangements for the homodimer of BmrA could then be suggested (Fig. 4d, blue and green circles). We ruled out the arrangement depicted in blue circles since, within a single row, the distance between a first dimer (light-blue circles) and a second dimer (dark-blue circles) of BmrA of 8.5 nm appeared too large to maintain the interactions between homodimers required for the stability of the membrane sheets. The other proposition (green circles) was consistent with a conformation of BmrA with NBDs separated by ~5 nm. Such distance between NBDs is larger than that found in P-gp but is the same as that reported for the open apo-MsbA from *E. coli* [9,21,22]. Interestingly, two recent reports have shown that, in the apo-conformation, the mouse P-gp in 3D crystals in detergent and MsbA in self-assembled β-sheet peptides can adopt different conformations with a different widening between the two NBDs [12,28]. Here, this suggests that BmrA also adopt at least two conformations with variable separation of NBDs in the lipid membranes.

Outward-facing conformation of BmrA with bound ADP-Vi

We also analyzed the nucleotide-bound state of BmrA. 2D crystallization trials were performed in the presence of ATP and orthovanadate (Vi), a specific inhibitor that blocks several ABC transporters including BmrA in an ADP-Vi post-hydrolytic conformation [8,29]. 2D trials by detergent removal in bulk led to small vesicles with densely packed but non-crystalline proteins (data not shown). However, 2D crystallization by the lipid layer method after specific binding of BmrA to a Ni^{2+}-NTA-DOGS lipid layer followed by detergent removal led to the formation of large and flat membranes of several microns with densely packed proteins (Fig. 5a). In these membranes, 2D crystalline arrays as large as 400 nm × 400 nm were found (Fig. 5b). A projection map of BmrA at 16 Å resolution was calculated from merged amplitudes and phases from four independent negatively stained 2D crystals with *p*2 symmetry (Tables S1 and S2). It is worth noting that the *p*2 symmetry indicates a unique orientation of the homodimeric BmrA in the reconstituted membrane

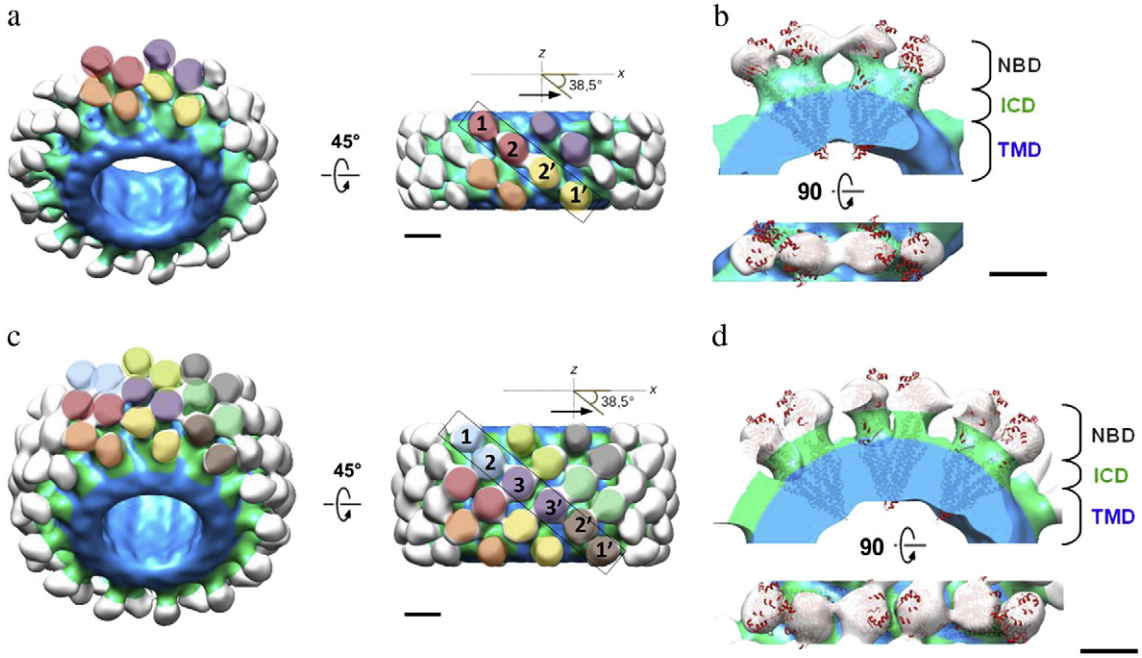

Fig. 2. 3D models of rings of BmrA in lipid membrane calculated with particles of *d*12 symmetry (a and b) or with particles of *d*13 symmetry (c and d). Homodimers of BmrA are lettered as (1, 2), (1′, 2′) and (3, 3′). Subdomains of BmrA, NBD (white), ICD (green) and membrane domain (blue). The mouse open apo-P-gp (in red; PDB code: 3G5U) was docked in densities of the homodimers of BmrA. Note that the TMD of P-gp is longer than BmrA because there is an insertion of 33 residues in the first extracellular loop of the P-gp between the transmembrane helices 1 and 2 (protruding toward the center of the ring). The bar represents 5 nm.

consistent with the specifically oriented binding to the lipid layer.

The projection map showed a bean-like molecule with two separated densities and a central depression with stain accumulation (Fig. 5c). Since the His_6-tag is present on the NBDs side of BmrA, one expects that the cytoplasmic side is facing the carbon-coated grid after the transfer. The opposite side, the extracellular side of BmrA, was then accessible to the negative staining. Thus, the two separated densities correspond to the extracellular helices bundles in an outward-facing conformation. The depression between the densities

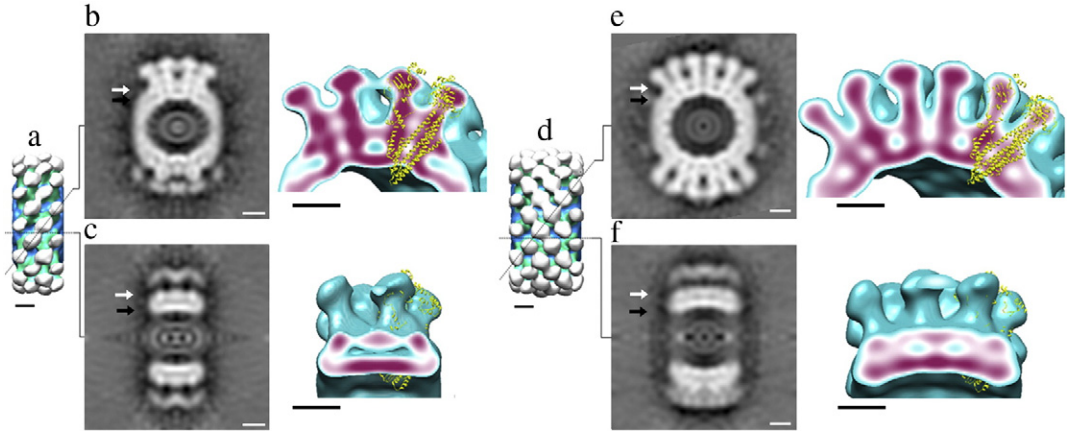

Fig. 3. TMDs of BmrA in the lipid bilayer. Slices through the *d*12 ring (a–c) and the *d*13 ring of BmrA (d–f). The slices along the constitutive row of homodimers of BmrA (b and e) revealed the internal structure of BmrA and the lipidic bilayer. The inner (black arrows) and outer (white arrows) leaflets of the lipid bilayer of the membrane are shown. The mouse open apo-P-gp (in yellow; PDB code: 3G5U) was docked in the densities of the homodimers of BmrA as in Fig. 2. The bars represent 5 nm.

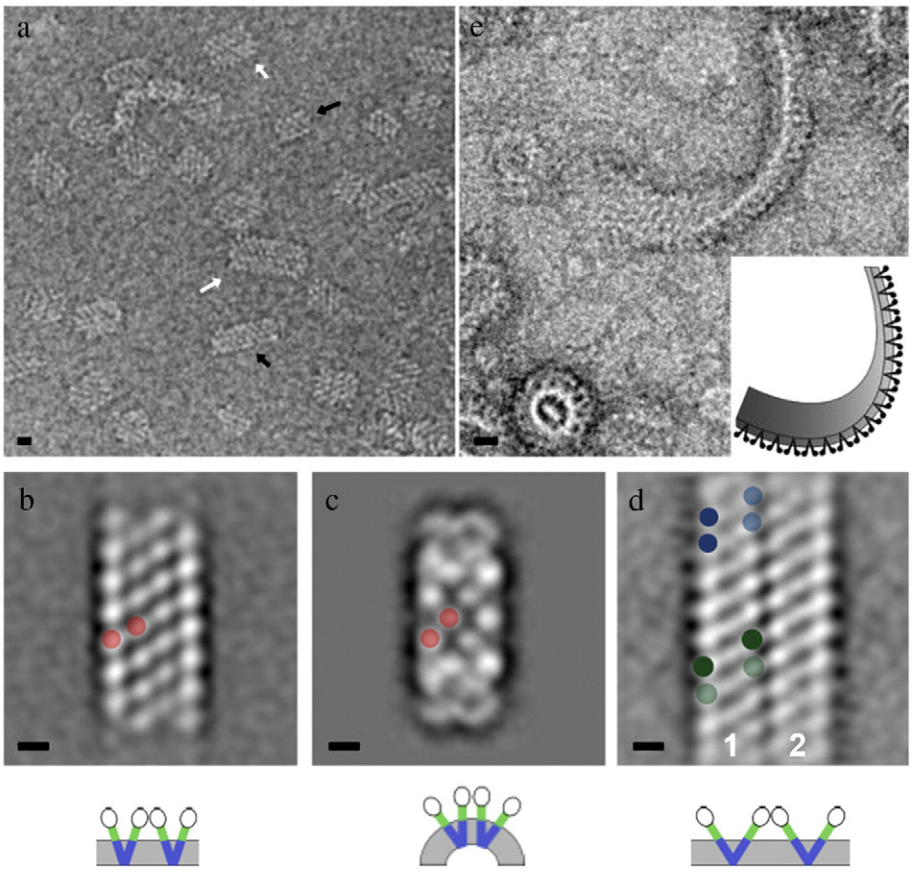

Fig. 4. Open apo-conformation of BmrA in membrane sheets. (a) cryo-EM of thin (black arrows) and large (white arrows) membrane sheets after binding to Ni^{2+}-NTA lipid layer. (b) Average image of thin membrane sheets. The NBDs of a homodimer of BmrA in a similar arrangement than in the *d*12 ring are highlighted (red circles). (c) Representative side view projection of *d*12 3D model and the arrangement of the homodimer of BmrA (red circles). (d) Average image of large membrane sheets constituted of two rows of proteins (numbered 1 and 2). Two possible arrangements of the homodimer of BmrA are depicted (green, blue circles). For each arrangement, two dimers are shown in light and dark color. The green-labeled dimers are the most likely arrangements (see the text). (e) Negatively stained imaged of large membrane sheets showing an asymmetrical insertion of BmrA in the membrane. The bars represent 5 nm.

was measured to be 1–2 nm deep on the same 2D crystals of BmrA by atomic force microscopy [30] and was consistent with the open outward-facing conformation as described for Sav1866 or MsbA (Fig. 5d).

Discussion

Here, we present two 3D models of BmrA in apo-conformation in lipid membrane and in a non-crystalline environment calculated from cryo-EM images (Figs. 2 and 3). Previous 3D reconstructions calculated from cryo-EM images have been obtained for MsbA in membrane in three nucleotide-bound states confirming a closed outward-facing conformation [31]. Several projection maps of the nucleotide-free mouse P-gp and a 3D model of nucleotide-bound P-gp at limited resolution and in negative staining have been calculated from 2D crystals [32,33].

In the 3D models of BmrA, the complete envelope and the main subdomains are well resolved. The catalytic domains NBDs are separated by 3 nm, two distinct bundles of TMDs are identified and both lipid leaflets of the membrane surrounding the protein are resolved (Figs. 2 and 3). Overall, the global conformation of BmrA is similar to the open apo-conformation of mouse or *C. elegans* P-gps [7,10].

The 3D model has been calculated from homogeneous ring-shaped assembly of 24 or 39 homodimers of BmrA. We have previously reported several pieces of evidence clearly supporting the view that BmrA in these rings adopts a native-like conformation [27,29]: (i) these rings were obtained regardless of the lipid composition including EPC/EPA as described here, *E. coli* lipids or synthetic lipids such as DMPC or dioleoyl-phosphatidylcholine (DOPC) or the detergent used during the reconstitution procedure; (ii) further

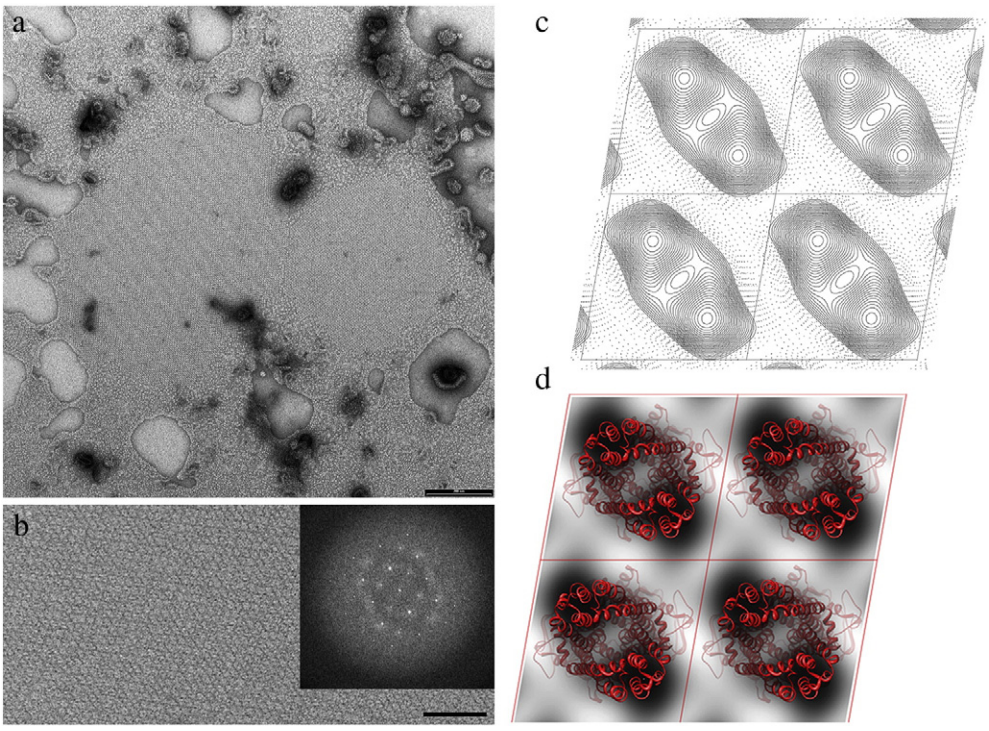

Fig. 5. 2D crystals of BmrA trapped in an ADP-Vi conformation. (a) Electron micrograph of membrane reconstituted BmrA after specific binding to a Ni^{2+}-NTA lipid layer. The scale bar represents 200 nm. (b) Negatively stained 2D crystals of BmrA. The scale bar represents 50 nm. Inset: Typical calculated power spectrum showing diffraction spots at 2 nm before image processing. (c) *p*2 symmetrized projection map calculated at 16 Å resolution. Densities above the mean and negative densities are indicated by continuous lines and dotted lines, respectively. The lattice parameters are a = 70 Å, b = 70 Å and γ = 101°. The unit cell, dark box, contains a homodimer of BmrA. Four unit cells are depicted. (d) Arrangement of molecules with overlaid X-ray structure of Sav1866 (PDB entry: 2HYD).

removal of the residual detergent molecules from the rings led to the coalescence of the rings to form tubes with the same diameter showing that the open conformation of BmrA was similar in the two supramacromolecular structures; and (iii) BmrA in these rings was capable to engage in a catalytic cycle, hydrolyzing ATP in a vanadate-sensitive manner, thereby leading to ring destruction that could not be analyzed further. Thus, these assemblies are transient and can be disrupted by the addition of nucleotide revealing that the intermolecular interactions are weak. Therefore, the transporter is not trapped in a dead-end conformation but is just waiting to bind and hydrolyze nucleotide, that is, in a native-like conformation competent for ATPase activity. Overall, it is clear that the rings are not due either to any non-native lipids or to remaining detergent molecules. Instead, the ring form is very likely imposed by the inherent ability of BmrA to adopt an open conformation in the resting state and in a lipidic environment. Thus, this strongly supports the view that the open apo-conformation of BmrA is a native-like conformation.

This conclusion seems to be at odds with our previous study where we used FRET to probe the conformation of BmrA in a lipidic environment [34]. However, at that time, the structures of MsbA that we used to estimate the distances between the two fluorescent probes were erroneous and were retracted soon after. Based on the Sav1866 [8] and mouse P-gp [7] published later on, and given the uncertainty inherent to the FRET distance calculations, it would have been impossible to discriminate between the two conformations of BmrA in our previous publication. The maximal variations in distances between the probes we used in 2005 were at most of 18 Å between the open and closed conformations. Here, the cryo-EM 3D models of BmrA have been calculated directly from images of BmrA without the need of pre-existing atomic structures and without labeling of specific amino acids.

BmrA was also present in another conformation where the NBDs were separated by ~5 nm (Fig. 4d), as found for open apo-*E. coli* MsbA [9]. BmrA is able to interact with, and possibly transport, several small-size P-gp substrates such as doxorubicin, rhodamine 6G and daunomycin and is inhibited by most P-gp inhibitors [18]. Moreover, overexpression of BmrA was found in cervimycin C-resistant clones of *B. subtilis*, suggesting that cervimycin C is also transported by BmrA [35]. Thus, to accommodate large substrates such as cervimycin (molecular mass, 1.3 kDa) or Kdo2-lipid A (molecular mass,

2.3 kDa) in the case of MsbA, these two transporters may sample wider conformations.

These two coexisting conformations are likely the most representative since they could have been classified and averaged. The presence of two conformation of BmrA is consistent with the large flexibility of the intracytoplasmic domains ICDs and NBDs of BmrA in the resting state reported from hydrogen/deuterium exchange experiments [25]. In the case of mouse and *C. elegans* P-gp in inward-facing conformations, five X-ray structures with different separations between NBDs have been described [7,10,12]. Large motions of the NBDs of P-gp were also found by molecular dynamic simulations and DEER [24]. Here, the two conformations of BmrA coexist in the same reconstituted sample while no other conformation was observed. Thus, although we cannot rule out that other minor conformations that could not be classified and averaged were also present in the sample, this suggest that these two conformations are the most stable. It is likely that lipid molecules contribute to the stabilization of these conformations. The ATPase activity of BmrA, like other ABC transporters, increased 5–10 times after reconstitution in membrane [18]. Moreover, negatively charged lipids with phosphatidic acid head group that we used for the formation of rings of BmrA have been suggested to enter into the cavity of P-gp and to stabilize the inward-facing conformation [36]. These conformations are not sensitive to the binding of substrates since we have previously shown that the addition of drugs such as doxorubicin, ATP alone (without Mg^{2+}) and ADP Mg^{2+}, added either after or during the formation of rings, has no effect on the structure of these rings [29]. This likely requires further analysis to at higher resolution but this is in line with the minor conformational changes reported for P-gp upon binding of specific inhibitors [7]. Finally, we do not found BmrA with its NBDs in contact in the apo-form, as reported for the X-ray structure of *Vibrio cholerae* MsbA [9] or for P-gp where a study by DEER indicated that a fraction of NBDs were in a closed-like conformation even in the absence of nucleotide [24].

The open conformation imposes an asymmetrical distribution of lipids in both leaflets to compensate the V-shape of BmrA. Indeed, the surface of lipid surrounding the cytoplasmic side of BmrA is larger than the extracellular side. Our data also show that the electron densities in both leaflets that are related to the chemical composition are different, with a possible accumulation of residual detergent molecules in the intracellular leaflet (cytoplasmic side) (Fig. 3). Since detergents are amphiphilic molecules known to stimulate or activate the ATPase activity of several ABC exporter [29,37], this suggests that substrates of BmrA may accumulate in the inner leaflet before being translocated.

Finally, a central question is whether the open inward state is functionally relevant. In *B. subtilis* and in actively growing cells, concentrations of ATP are in the millimolar range (1.5–3 mM) [38]. Starving or stressful conditions have been shown to dramatically reduce the ATP level in plant [39], yeast [40], bacteria (from ~100 pM down to even 0.1 pM) [41] or even mammal cells [42]. In *Bacillus* species, dreadful conditions trigger the formation of spores where the ATP level drops considerably (about 250-fold less ATP in the spores than the vegetative cells) [43]. Therefore, at least in "extreme" conditions that are nevertheless prevalent in the natural habitat of all microorganisms, the ABC transporters are facing a constant "lack" of energy and thus will often return to their resting state, that is, with their NBDs free of nucleotides in an open inward-facing conformation. Thus, in the wild and for microorganisms, the resting state with empty NBDs is certainly a common, physiological, conformation of ABC transporters.

Materials and Methods

Materials

EPC, EPA, DOPC and Ni-nitrilotriacetic-1,2-dioleoyl-sn-glycero-3-{[*N*(5-amino-1-carboxypentyl)iminodiacetic acid] succinyl} (Ni^{2+}-NTA-DOGS) were of the highest purity available and purchased from Avanti Polar Lipids. *N*-Dodecyl-β-D-maltoside (DDM) was purchased from Anatrace.

His_6-BmrA from *B. subtilis* were expressed in *E. coli* and purified in DDM according to Ref. [18]. Aliquots of 50 µl of preparations were kept frozen before use at −80 °C at 1–1.5 mg/ml protein concentration in 50 mM Tris (pH 8), 50 mM NaCl, 5 mM β-mercaptoethanol, 0.05% DDM and 10% glycerol.

Reconstitution of BmrA in inward-facing apo-conformation

BmrA ring-like structures were formed according to the procedure previously described [27]. Briefly, purified BmrA in 50 mM Hepes (pH 7.5) and 150 mM KCl at 0.5 mg/ml was mixed with a mixture of EPC/EPA (9/1 mol/mol) at a lipid-to-protein ratio of 1.2 (w/w) in the presence of 0.2% DDM. After 1-h incubation at room temperature, the micellar solution was treated with 40 mg Bio-Beads per milliliter. The solution was withdrawn after 45 min of incubation with Bio-Beads, leading to a homogeneous preparation of ring-like structures that were stable for several days at 4 °C. Alternatively, detergent was removed by addition of β-cyclodextrins and rings were formed at a β-cyclodextrin-to-DDM ratio of 1.18 mol/mol [44].

Cryo-electron images of the rings were obtained after specific binding to a functionalized lipid layer with Ni^{2+}-NTA-DOGS. Briefly, 0.5 µl of Ni^{2+}-NTA-DOGS solution (0.1 mM) was spread at the air/water interface of homemade Teflon wells [45]. Then DDM was injected below the lipid layer at 0.75 mM final concentration under stirring. After 5 min, 6 µl of ring-like structures was injected below the lipid layer for 30 min of incubation under stirring.

The surface was picked up with holey formvar carbon grids (Ted Pella, Inc., USA) and flash-frozen in liquid ethane.

2D crystallization of ADP-Vi trapped BmrA

2D crystallization trials were performed using the lipid layer strategy according to Refs. [45] and [46]. Protein at 0.25 mg/ml in 50 mM Tris (pH 8), 5 mM $MgCl_2$, 150 mM KCl and 0.5% DDM was supplemented with EPC/EPA lipid mixture at 0.4–0.6 (w/w) lipid-to-protein ratio and equilibrated for 2 h at 4 °C. A lipid layer constituted by mixture of Ni^{2+}-NTA-DOGS/DOPC (1:1 mol/mol) and 0.5 µl of a 0.1 mM lipid solution in $CHCl_3$/CHOH 9/1 (v/v) was spread at the air/water interface of Teflon wells. Then 6 µl of the lipid/protein/detergent was injected through a side hole in a 60-µl Teflon well below the functionalized lipid layer. Binding was carried for 5 h at 4 °C under slow stirring. Detergent was removed by addition of 2.5 mg of Bio-Beads though the side hole of the well and reconstitution was performed during 2 days at 4 °C without stirring. To block BmrA in ADP-Vi state, we included 2.5 mM orthovanadate and 5 mM ATP in the crystallization buffer during the binding step.

Electron microcopy

Grids of BmrA in open inward-facing conformation were transferred into a FEI CM200 FEG electron microscope operating at 200 kV at nominal magnification of 50,000×. Micrographs were recorded on SO163 films and digitized with a Nikon Coolscan 8000 at 2.5 Å/pixel.

Grids of 2D crystals of the ADP-Vi trapped His_6-BmrA formed at the lipid layer surface were picked up with carbon-coated grids and stained with 1% uranyl acetate. Electron micrographs were taken under low-dose mode on a Phillips CM120 microscope operating at 120 kV at a nominal magnification of 45,000× using a 1024 × 1024 pixel SSC Gatan CCD camera. The defocus ranged from −0.2 µm to −1 µm. The pixel size, calibrated using bacteriorhodopsin 2D crystals, was 3.86 ± 0.1 Å.

Image processing: 3D model of *d*12 and *d*13 ring of BmrA in apo-conformation

Image processing was performed using Xmipp 2.4 suite [47–49]. A set of 102 micrographs selected on their power spectrum quality after contrast inversion was analyzed. The defocus values and the parameters of the envelope function parameters were modeled and manually controlled. Next, micrographs were phase-flipped according to the CTF parameters.

For the 3D reconstruction of the *d*12 and *d*13 volumes, a total number of 2158 projections with shapes and sizes compatible with the previous 3D model of the ring of BmrA [27] were windowed into 200 × 200 pixel box using Boxer software. Images were centered, normalized and band-pass filtered between 10 Å (2× Nyquist frequency) and 200 Å before classification. A hierarchical clustering approach using correntropy (CL2D) [49] was performed over images imposing 20 final classes average over 20 iterations (Fig. S2). A 2D rotational analysis was performed to identify symmetries within each class. Before angular assignment, a raised-cosine mask was applied to particles. A circular mask of 180 pixel diameter, a rectangular mask of 180 × 90 pixel and a rectangular mask of 180 × 120 pixel were used for the circular ring-shaped views, the small rectangular view and the large rectangular view, respectively. Twenty cycles of projection matching angular refinement coupled to Fourier inverse 3D reconstruction [49] and amplitude correction were performed. A synthetic ring volume of 40 nm diameter and 17.5 nm width and a hole of 9 nm diameter were used as initial reference (Fig. S2) and *d*12 or *d*13 symmetry was applied for *d*12 or *d*13 3D models, respectively (Figs. S3 and S4). The final resolutions of the *d*12 and *d*13 3D reconstructions were estimated to 23 Å and 25 Å from the FSC (*F*ourier *s*hell *c*orrelation) curve using the FSC = 0.5 cutoff criteria. Atomic structure of mouse P-gp (PDB entry: 3G5U) was filtered at 23 Å or 25 Å and fitted into the 3D maps using UCSF Chimera and Situs software. Note that the TMD of P-gp is longer than BmrA because there is an insertion of 33 residues in the first extracellular loop of the P-gp between the transmembrane helices 1 and 2 (protruding toward the center of the ring). Further details on the image processing are described in the supplementary information.

For the 2D analysis of the tubes of BmrA, 2D analysis, 198 images of large tubes and 162 images of thin tubes were selected and boxed in 200 × 200 pixel box using Boxer software. Images were centered, normalized and band-pass filtered between 10 Å (2× Nyquist frequency) and 200 Å before alignment. Each group of tubes was aligned using 2D free-reference alignment algorithm. Resolution was estimated to be about 30 Å in both cases based on 0.5 FSC criteria.

Projection map of BmrA trapped in ADP-Vi conformation

The projection map of BmrA trapped in ADP-Vi conformation was calculated with 2dx package (release 3.0.03), which included two cycles of lattice unbending (CCUNBENDK), calculation of defocus and astigmatism values (CTFFIND) and correction of the contrast Fourier transform (CTFAPPLY) [50]. Plane symmetry was established by analysis of the images using ALL SPACE with IQ 1–4 up to 15 Å. The four best images ranging in defocus from −0.4 to −0.8 µm were merged and used to calculate a projection map at 16 Å resolution with a *p*2 symmetry (see Tables S1 and S2).

Accession numbers

EmDep deposition has been assigned EMDataBank Accession Code EMD-5525 for the *d*12 map entry and EMD-5526 for the *d*13 map entry.

Acknowledgments

We thank A. Di Cicco and J. Manzi for technical support. We thank Dr. J. Busselez for fruitful discussion and Dr. H. Stahlberg and Dr. A. Engel for their continuous support. This work was supported by Institut Curie and Centre National de la Recherche

Scientifique and by the Agence Nationale de la Recherche Grant No. ANR-06-Blan-0420 (to D.L. and J.M.J.).

Competing Financial Interest: The authors declare no financial competing interests.

Appendix A. Supplementary data

Supplementary data to this article can be found online at http://dx.doi.org/10.1016/j.jmb.2014.03.002.

Received 7 August 2013;
Received in revised form 1 March 2014;
Accepted 4 March 2014
Available online 11 March 2014

Keywords:
ABC transporter;
inward-facing conformation;
electron microscopy;
conformation in lipid bilayer;
BmrA

Present address: F. Gubellini, Institut Pasteur, Unité G5 Biologie Structurale de la Sécrétion Bactérienne, Bâtiment Metchnikoff, 25–28 rue du Docteur Roux, 75015 Paris, France.
Present address: J.-M. Jault, UMR 5086, CNRS/UCBLyon 1, 7 Passage du Vercors, 69376 Lyon Cedex 07, France.

Abbreviations used:
DDM, N-dodecyl-β-d-maltoside; EPC, egg phosphatidylcholine; EPA, egg phosphatidic acid; DOPC, dioleoylphosphatidylcholine; cryo-EM, cryo-electron microscopy; 3D, three-dimensional; TMD, transmembrane domain; LRET, luminescence resonance energy transfer; DEER, double electron–electron resonance; FRET, fluorescence resonance energy transfer.

References

[1] Rees DC, Johnson E, Lewinson O. ABC transporters: the power to change. Nat Rev Mol Cell Biol 2009;10:218–27.
[2] Davidson AL, Dassa E, Orelle C, Chen J. Structure, function, and evolution of bacterial ATP-binding cassette systems. Microbiol Mol Biol Rev 2008;72:317–64.
[3] Higgins CF. Multiple molecular mechanisms for multidrug resistance transporters. Nature 2007;446:749–57.
[4] Locher KP. Review: structure and mechanism of ATP-binding cassette transporters. Philos Trans R Soc London Ser B 2009;364:239–45.
[5] Parcej D, Tampe R. ABC proteins in antigen translocation and viral inhibition. Nat Chem Biol 2010;6:572–80.
[6] Zolnerciks JK, Andress EJ, Nicolaou M, Linton KJ. Structure of ABC transporters. Essays Biochem 2011;50:43–61.
[7] Aller SG, Yu J, Ward A, Weng Y, Chittaboina S, Zhuo R, et al. Structure of P-glycoprotein reveals a molecular basis for poly-specific drug binding. Science 2009;323:1718–22.
[8] Dawson RJ, Locher KP. Structure of a bacterial multidrug ABC transporter. Nature 2006;443:180–5.
[9] Ward A, Reyes CL, Yu J, Roth CB, Chang G. Flexibility in the ABC transporter MsbA: alternating access with a twist. Proc Natl Acad Sci U S A 2007;104:19005–10.
[10] Jin MS, Oldham ML, Zhang Q, Chen J. Crystal structure of the multidrug transporter P-glycoprotein from *Caenorhabditis elegans*. Nature 2012;490:566–9.
[11] Shintre CA, Pike AC, Li Q, Kim JI, Barr AJ, Goubin S, et al. Structures of ABCB10, a human ATP-binding cassette transporter in apo- and nucleotide-bound states. Proc Natl Acad Sci U S A 2013;110:9710–5.
[12] Ward AB, Szewczyk P, Grimard V, Lee CW, Martinez L, Doshi R, et al. Structures of P-glycoprotein reveal its conformational flexibility and an epitope on the nucleotide-binding domain. Proc Natl Acad Sci U S A 2013. http://dx.doi.org/10.1073/pnas.1309275110.
[13] Higgins CF, Linton KJ. The ATP switch model for ABC transporters. Nat Struct Mol Biol 2004;11:918–26.
[14] George AM, Jones PM. Perspectives on the structure–function of ABC transporters: the Switch and Constant Contact models. Prog Biophys Mol Biol 2012;109:95–107.
[15] Kerr ID, Jones PM, George AM. Multidrug efflux pumps: the structures of prokaryotic ATP-binding cassette transporter efflux pumps and implications for our understanding of eukaryotic P-glycoproteins and homologues. FEBS J 2010;277:550–63.
[16] Gottesman MM, Ambudkar SV, Xia D. Structure of a multidrug transporter. Nat Biotechnol 2009;27:546–7.
[17] Eckford PD, Sharom FJ. Functional characterization of *Escherichia coli* MsbA: interaction with nucleotides and substrates. J Biol Chem 2008;283:12840–50.
[18] Steinfels E, Orelle C, Fantino JR, Dalmas O, Rigaud JL, Denizot F, et al. Characterization of YvcC (BmrA), a multidrug ABC transporter constitutively expressed in *Bacillus subtilis*. Biochemistry 2004;43:7491–502.
[19] Verhalen B, Wilkens S. P-glycoprotein retains drug-stimulated ATPase activity upon covalent linkage of the two nucleotide binding domains at their C-terminal ends. J Biol Chem 2011;286:10476–82.
[20] Cooper RS, Altenberg GA. Association/dissociation of the nucleotide-binding domains of the ATP-binding cassette protein MsbA measured during continuous hydrolysis. J Biol Chem 2013;288:20785–96.
[21] Zou P, McHaourab HS. Alternating access of the putative substrate-binding chamber in the ABC transporter MsbA. J Mol Biol 2009;393:574–85.
[22] Zou P, Bortolus M, McHaourab HS. Conformational cycle of the ABC transporter MsbA in liposomes: detailed analysis using double electron-electron resonance spectroscopy. J Mol Biol 2009;393:586–97.
[23] Zou P, Mchaourab H. Increased sensitivity and extended range of distance measurements in spin-labeled membrane proteins: Q-band double electron-electron resonance and nanoscale bilayers. Biophys J 2010;98:L18–20.
[24] Wen PC, Verhalen B, Wilkens S, McHaourab HS, Tajkhorshid E. On the origin of large flexibility of P-glycoprotein in the inward-facing state. J Biol Chem 2013;288:19211–20.
[25] Mehmood S, Domene C, Forest E, Jault JM. Dynamics of a bacterial multidrug ABC transporter in the inward- and outward-facing conformations. Proc Natl Acad Sci U S A 2012;109:10832–6.

[26] Hirst SJ, Alexander N, McHaourab HS, Meiler J. RosettaEPR: an integrated tool for protein structure determination from sparse EPR data. J Struct Biol 2011;173:506–14.
[27] Chami M, Steinfels E, Orelle C, Jault JM, Di Pietro A, Rigaud JL, et al. Three-dimensional structure by cryo-electron microscopy of YvcC, an homodimeric ATP-binding cassette transporter from *Bacillus subtilis*. J Mol Biol 2002;315:1075–85.
[28] Tao H, Lee SC, Moeller A, Roy RS, Siu FY, Zimmermann J, et al. Engineered nanostructured beta-sheet peptides protect membrane proteins. Nat Methods 2013;10:759–61.
[29] Orelle C, Gubellini F, Durand A, Marco S, Levy D, Gros P, et al. Conformational change induced by ATP binding in the multidrug ATP-binding cassette transporter BmrA. Biochemistry 2008;47:2404–12.
[30] Seantier B, Dezi M, Gubellini F, Berquand A, Godefroy C, Dosset P, et al. Transfer on hydrophobic substrates and AFM imaging of membrane proteins reconstituted in planar lipid bilayers. J Mol Recognit 2011;24:461–6.
[31] Ward A, Mulligan S, Carragher B, Chang G, Milligan RA. Nucleotide dependent packing differences in helical crystals of the ABC transporter MsbA. J Struct Biol 2009;165:169–75.
[32] Lee JY, Urbatsch IL, Senior AE, Wilkens S. Projection structure of P-glycoprotein by electron microscopy. Evidence for a closed conformation of the nucleotide binding domains. J Biol Chem 2002;277:40125–31.
[33] Lee JY, Urbatsch IL, Senior AE, Wilkens S. Nucleotide-induced structural changes in P-glycoprotein observed by electron microscopy. J Biol Chem 2008;283:5769–79.
[34] Dalmas O, Do Cao MA, Lugo MR, Sharom FJ, Di Pietro A, Jault JM. Time-resolved fluorescence resonance energy transfer shows that the bacterial multidrug ABC half-transporter BmrA functions as a homodimer. Biochemistry 2005;44:4312–21.
[35] Krugel H, Licht A, Biedermann G, Petzold A, Lassak J, Hupfer Y, et al. Cervimycin C resistance in *Bacillus subtilis* is due to a promoter up-mutation and increased mRNA stability of the constitutive ABC-transporter gene bmrA. FEMS Microbiol Lett 2010;313:155–63.
[36] Marcoux J, Wang SC, Politis A, Reading E, Ma J, Biggin PC, et al. Mass spectrometry reveals synergistic effects of nucleotides, lipids, and drugs binding to a multidrug resistance efflux pump. Proc Natl Acad Sci U S A 2013;110:9704–9.
[37] Li-Blatter X, Nervi P, Seelig A. Detergents as intrinsic P-glycoprotein substrates and inhibitors. Biochim Biophys Acta 2009;1788:2335–44.
[38] Matsuno K, Blais T, Serio AW, Conway T, Henkin TM, Sonenshein AL. Metabolic imbalance and sporulation in an isocitrate dehydrogenase mutant of *Bacillus subtilis*. J Bacteriol 1999;181:3382–91.
[39] Shimano F, Ashihara H. Effect of long-term phosphate starvation on the levels and metabolism of purine nucleotides in suspension-cultured *Catharanthus roseus* cells. Phytochemistry 2006;67:132–41.
[40] Thomsson E, Svensson M, Larsson C. Rapamycin pretreatment preserves viability, ATP level and catabolic capacity during carbon starvation of Saccharomyces cerevisiae. Yeast 2005;22:615–23.
[41] Ganesan B, Stuart MR, Weimer BC. Carbohydrate starvation causes a metabolically active but nonculturable state in *Lactococcus lactis*. Appl Environ Microbiol 2007;73:2498–512.
[42] Kriat M, Fantini J, Vion-Dury J, Confort-Gouny S, Galons JP, Cozzone PJ. Energetic metabolism of glucose, mannose and galactose in glucose-starved rat insulinoma cells anchored on microcarrier beads. A phosphorus-31 NMR study. Biochimie 1992;74:949–55.
[43] Setlow P, Kornberg A. Biochemical studies of bacterial sporulation and germination. XXII. Energy metabolism in early stages of germination of *Bacillus megaterium* spores. J Biol Chem 1970;245:3637–44.
[44] Signorell GA, Kaufmann TC, Kukulski W, Engel A, Remigy HW. Controlled 2D crystallization of membrane proteins using methyl-beta-cyclodextrin. J Struct Biol 2007;157:321–8.
[45] Levy D, Mosser G, Lambert O, Moeck GS, Bald D, Rigaud JL. Two-dimensional crystallization on lipid layer: a successful approach for membrane proteins. J Struct Biol 1999;127:44–52.
[46] Dezi M, Fribourg PF, Di Cicco A, Jault JM, Chami M, Levy D. Binding, reconstitution and 2D crystallization of membrane or soluble proteins onto functionalised lipid layer observed in situ by reflected light microscopy. J Struct Biol 2011;174:307–14.
[47] Sorzano CO, Marabini R, Velazquez-Muriel J, Bilbao-Castro JR, Scheres SH, Carazo JM, et al. XMIPP: a new generation of an open-source image processing package for electron microscopy. J Struct Biol 2004;148:194–204.
[48] Scheres SH, Nunez-Ramirez R, Sorzano CO, Carazo JM, Marabini R. Image processing for electron microscopy single-particle analysis using XMIPP. Nat Protoc 2008;3:977–90.
[49] Sorzano CO, Bilbao-Castro JR, Shkolnisky Y, Alcorlo M, Melero R, Caffarena-Fernandez G, et al. A clustering approach to multireference alignment of single-particle projections in electron microscopy. J Struct Biol 2010;171:197–206.
[50] Gipson B, Zeng X, Zhang ZY, Stahlberg H. 2dx—user-friendly image processing for 2D crystals. J Struct Biol 2007;157:64–72.